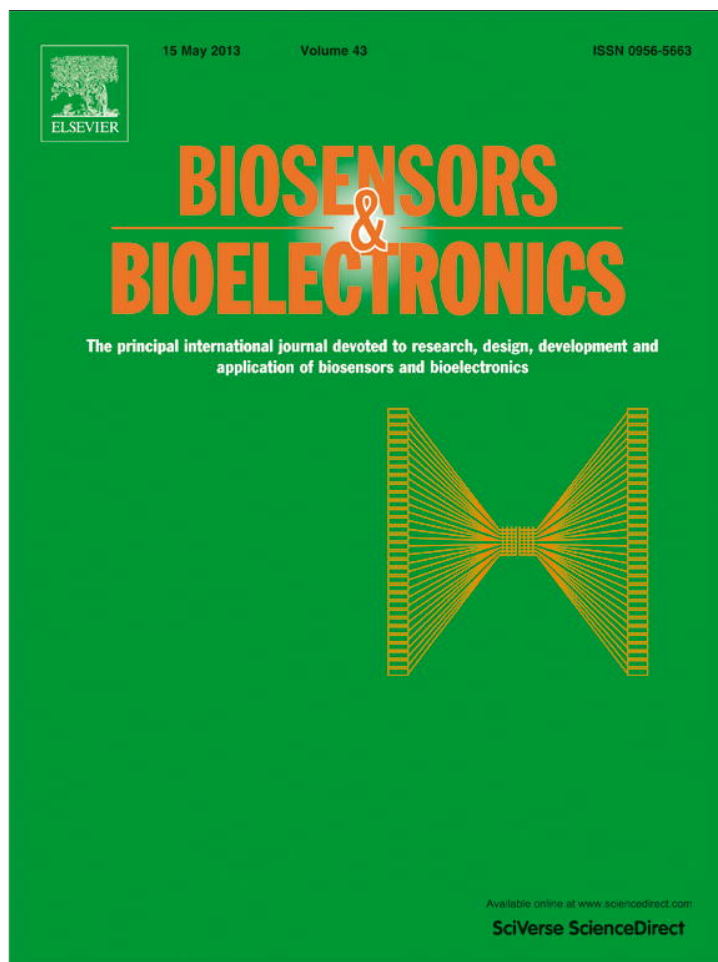


Provided for non-commercial research and education use.
Not for reproduction, distribution or commercial use.



This article appeared in a journal published by Elsevier. The attached copy is furnished to the author for internal non-commercial research and education use, including for instruction at the authors institution and sharing with colleagues.

Other uses, including reproduction and distribution, or selling or licensing copies, or posting to personal, institutional or third party websites are prohibited.

In most cases authors are permitted to post their version of the article (e.g. in Word or Tex form) to their personal website or institutional repository. Authors requiring further information regarding Elsevier's archiving and manuscript policies are encouraged to visit:

<http://www.elsevier.com/copyright>

Contents lists available at [SciVerse ScienceDirect](http://www.sciencedirect.com)

Biosensors and Bioelectronics

journal homepage: www.elsevier.com/locate/bios

Bloch surface wave-enhanced fluorescence biosensor

Koji Toma^a, Emiliano Descrovi^b, Mana Toma^a, Mirko Ballarini^b, Pietro Mandracci^b,
Fabrizio Giorgis^b, Anca Mateescu^c, Ulrich Jonas^{c,d}, Wolfgang Knoll^{a,e}, Jakub Dostálek^{a,*}^a AIT—Austrian Institute of Technology GmbH, BioSensor Technologies, Muthgasse 11, 1190 Vienna, Austria^b Dipartimento di Scienza Applicata e Tecnologia, Politecnico di Torino, C.so Duca degli Abruzzi 24, 10129 Torino, Italy^c FORTH/IESL, BOMCLab, Voutes Street 1527, 71110 Heraklion, Greece^d Macromolecular Chemistry, University of Siegen, Department Chemistry–Biology, Adolf-Reichwein-Strasse 2, Siegen 57076, Germany^e Nanyang Technological University, Centre for Biomimetic Sensor Science 637553, Singapore

ARTICLE INFO

Article history:

Received 24 August 2012

Received in revised form

7 November 2012

Accepted 1 December 2012

Available online 8 December 2012

Keywords:

Bloch surface wave
Enhanced fluorescence
Bragg mirror
Photonic crystal
Biosensor
Immunoassay

ABSTRACT

A new approach to signal amplification in fluorescence-based assays for sensitive detection of molecular analytes is reported. It relies on a sensor chip carrying a one-dimensional photonic crystal (1DPC) composed of two piled up segments which are designed to increase simultaneously the excitation rate and the collection efficiency of fluorescence light. The top segment supports Bloch surface waves (BSWs) at the excitation wavelength and the bottom segment serves as a Bragg mirror for the emission wavelength of used fluorophore labels. The enhancement of the excitation rate on the sensor surface is achieved through the resonant coupling to BSWs that is associated with strong increase of the field intensity. The increasing of collection efficiency of fluorescence light emitted from the sensor surface is pursued by using the Bragg mirror that minimizes its leakage into a substrate and provides its beaming toward a detector. In order to exploit the whole evanescent field of BSW, extended three-dimensional hydrogel-based binding matrix that is functionalized with catcher molecules is attached to 1DPC for capturing of target analyte from a sample. Simulations supported by experiments are presented to illustrate the design and determined the performance characteristics of BSW-enhanced fluorescence spectroscopy. A model immunoassay experiment demonstrates that the reported approach enables increasing signal to noise ratio, resulting in about one order of magnitude improved limit of detection (LOD) with respect to regular total internal reflection fluorescence (TIRF) configuration.

© 2012 Elsevier B.V. All rights reserved.

1. Introduction

Over the last decade, we witnessed growing needs for advanced tools enabling detection of trace amounts of chemical and biological analytes with improved sensitivity and shortened analysis time in important areas of medical diagnostics (Giljohann and Mirkin, 2009) and food control (Lazcka et al., 2007). In the field of analytical technologies relying on fluorescence which represents one of the mostly used methods, plasmon-enhanced fluorescence (PEF) offers an attractive means to address these challenges. This approach provides strong amplification of fluorescence signal through the enhanced electromagnetic field intensity originating from collective oscillations of electron density at metallic surfaces (Ford and Weber, 1984; Giannini et al., 2010). A number of advanced assays and biological studies have been carried out by taking advantage of enhanced

fluorescence excitation via surface plasmons at wavelength matching the fluorophore absorption band and by using directional surface plasmon-coupled emission occurring at the fluorescence emission wavelength (Dostálek and Knoll, 2008; Fort and Grésillon, 2008; Garcia-Parajo, 2008; Lakowicz et al., 2008; Neumann et al., 2002).

Bloch surface waves (BSWs) supported by one-dimensional dielectric photonic crystals (1DPC) were shown to exhibit similar characteristics to surface plasmons (Descrovi et al., 2008; Robertson, 1999) and they were proposed for application in optical sensors (Guo et al., 2010; Rivolo et al., 2012; Robertson and May, 1999; Shinn and Robertson, 2005). The field of BSWs exhibits an envelope that evanescently decays from the 1DPC surface into the substrate and top dielectric. With respect to surface plasmons, the field profile and dispersion relation of BSWs can be flexibly controlled through the design of 1DPC and high-Q resonances were reported due to low absorption coefficients of 1DPC dielectric layers (Farmer et al., 2012; Sinibaldi et al., 2012). In addition, the use of dielectric materials avoids undesired Förster resonance energy transfer, which strongly quenches the

* Corresponding author. Tel.: +43 50550 4470; fax: +43 50550 4450.
E-mail address: jakub.dostalek@ait.ac.at (J. Dostálek).

fluorescence signal at close proximity to metals in plasmon-enhanced fluorescence schemes. Similarly to surface plasmon-enhanced fluorescence, the amplification of fluorescence signal originating from fluorophores attached to 1DPC structures was proposed based on the enhanced field intensity associated to BSWs (Ballarini et al., 2011).

This paper aims at a new type of planar 1DPC structure that improves the sensitivity of fluorescence assays by the combination of three mechanisms. Firstly, the enhancement of the excitation rate of fluorophore labels by resonantly excited BSW is pursued. Secondly, the profile of the evanescent field of BSW is tuned in order to probe larger distances from the surface at which a three-dimensional hydrogel-binding matrix is attached in order to capture higher amounts of target analyte molecules. Thirdly, the fluorescence light that is accompanied with affinity binding of target analyte is collected with high efficiency by minimizing its leakage into the substrate and by the enhancing the intensity emitted toward a detector located in front of the sensor chip. The potential of the developed 1DPC with a large-binding capacity hydrogel matrix for the amplification of fluorescence signal in fluorescence-based assays is demonstrated in a model immunoassay experiment. Achieved performance characteristics are compared to the same assay with regular total internal reflection fluorescence (TIRF) readout and obtained results reveal an order of magnitude improved limit of detection.

2. Materials and methods

2.1. Materials

Polymer SU-8 2000.5 was purchased from Microchem (USA). Phosphate buffered saline (PBS, 140 mM NaCl, 10 mM phosphate, 3 mM KCl, and a pH of 7.4) was obtained from Calbiochem (Germany). PBS-Tween (PBS-T) was prepared by adding 0.05% of Tween 20 (Sigma-Aldrich, USA) to PBS solution. Mouse immunoglobulin G (mIgG) and an antibody specific for this analyte (a-mIgG) were from Molecular Probes (USA). a-mIgG was labeled with Alexa Fluor 647 dye with the dye-to-protein molar ratio of 4.5. This dye exhibits the absorption and emission wavelengths of $\lambda_{ab}=650$ nm and $\lambda_{em}=668$ nm, respectively. 10 mM acetate buffer (ACT) with pH=4 was prepared in house. 1-Ethyl-3-(3-dimethylaminopropyl) carbodiimide (EDC) was purchased from Pierce (USA) and ethanolamine was purchased from Sigma-Aldrich (USA). Photocrosslinked poly(N-isopropylacrylamide) (NIPAAm)-based hydrogel and sodium para-tetrafluorophenol sulfonate (TFPS) were synthesized as described in our previous work (Aulasevich et al., 2009; Beines et al., 2007). The hydrogel was composed of the terpolymer with N-isopropylacrylamide, methacrylic acid, and 4-methacryloyl benzophenone. The methacrylic acid allows the post-modification of the hydrogel by protein molecules and benzophenone moieties serve for the polymer network photo-crosslinking.

2.2. Photonic structure layout and fabrication

The 1DPC structure presented in Fig. 1(a) was prepared for BSW-enhanced fluorescence studies on a BK7 glass substrate by sequential plasma-enhanced chemical vapor deposition (PECVD) of hydrogenated silicon nitride $Si_{1-x}N_x:H$ layers. The refractive index of each layer was tuned by adjusting the nitrogen content x through the control of the ammonia fraction in the SiH_4+NH_3 plasma. In the PECVD process, the substrate temperature and the electrode distance were set to 220 °C and 20 mm, respectively. A total pressure of 0.45 Torr and a RF power density of 21 mW/cm² were used. The reactive gas flow ratio $[NH_3]/([SiH_4]+[NH_3])$ was

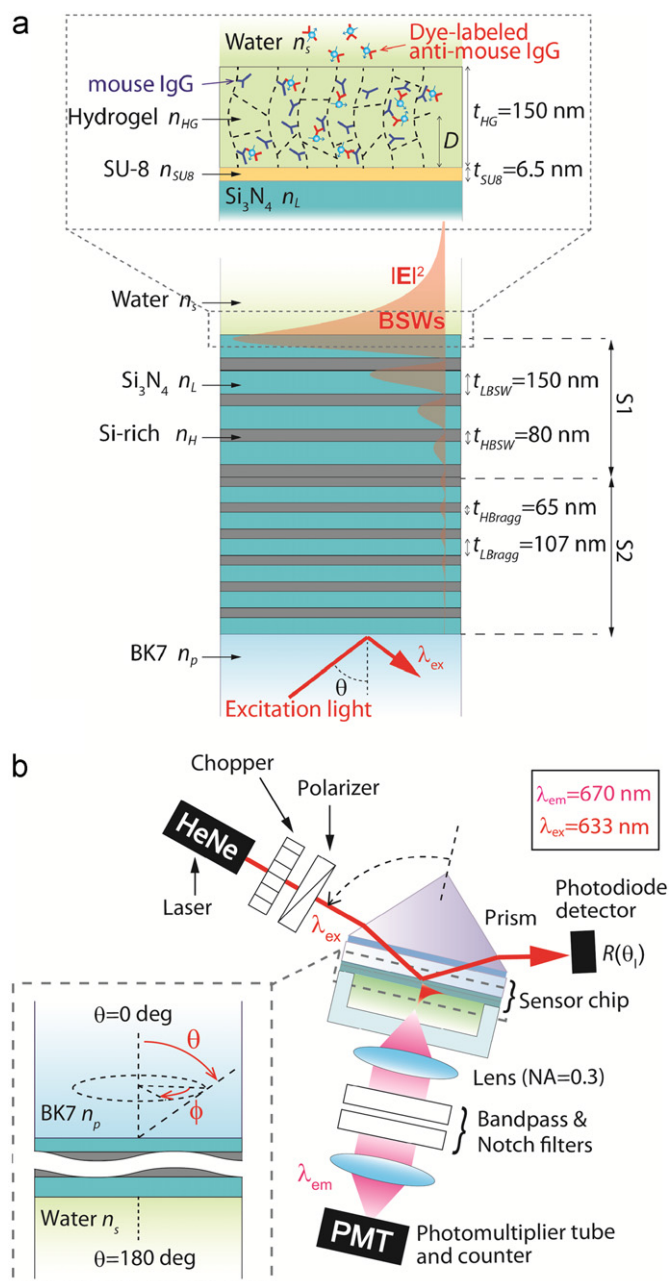


Fig. 1. (a) 1DPC composed of two segments of periodic low and high refractive index layers designed to support BSWs (S1) and serve as Bragg mirror (S2) with attached hydrogel binding matrix for the capture of target analyte; (b) Experimental setup for Bloch surface wave-enhanced fluorescence spectroscopy.

operated at 95 for the stoichiometric silicon nitride and at 53 for Si-rich silicon nitride layers. The 1DPC structure was composed of two segments S1 and S2 that are constituted by a periodic stack of high (Si-rich, under-stoichiometric amorphous silicon nitride) and low (Si_3N_4 , stoichiometric silicon nitride) refractive index (RI) layers. The top segment S1 was designed to support BSWs and it comprises four pairs of high and low RI layers with the thickness of $t_{HBSW}=80$ nm and $t_{LBSW}=150$ nm, respectively. The bottom segment S2 was designed to function as a Bragg mirror and it carries five pairs of high and low refractive index layers with a thickness of $t_{HBragg}=65$ nm and $t_{LBragg}=107$ nm, respectively. Let us note that the thickness of each prepared layer was typically controlled with the accuracy of several per cent. This gives rise to a random (Gaussian) distribution of layer thicknesses across the

multilayer stack. The thickness and refractive index of layers were determined by spectroscopic analysis of individual homogeneous films (Cary 500 UV-VIS-NIR spectrometer, Varian, USA).

2.3. Functionalization of sensor chip

The sensor chips for BSW-enhanced fluorescence (carrying 1DPC on BK7 glass) and TIRF (bare BK7 glass) were identically functionalized by using the following protocol. Firstly, a SU-8 with the thickness of $t_{\text{SU8}}=6.5$ nm was deposited by spin coating from 3 vol% solution in order to serve as a linker layer. The thickness of SU-8 smaller than 10 nm was chosen in order to attach the NIPAAm-based hydrogel film as close to the 1DPC surface as possible and thus achieve the maximum overlap with the BSW field. NIPAAm-based polymer (dissolved in ethanol at the concentration of 4 mg/mL) was spincoated on the SU-8 surface followed by overnight drying and exposing to UV light (irradiation dose of 5 J/cm^2 at a wavelength of $\lambda=365$ nm). The UV light simultaneously crosslinked and attached the NIPAAm polymer network to the surface by using polymer-bound benzo-phenon groups. The dry hydrogel film thickness of 16 nm was measured by surface plasmon resonance spectroscopy. In order to immobilize mIgG molecules into the polymer network, a protocol reported previously by our group was used (Aulasevich et al., 2009). Briefly, the hydrogel film was swollen in ACT buffer and its carboxylic groups were activated by the incubation with a mixture of EDC (37.5 mg mL^{-1}) and TFPS (10.5 mg mL^{-1}) dissolved in water. Then, the mIgG was diffused into the hydrogel from ACT buffer and reacted with active ester moieties via their amine groups. Finally, un-reacted active ester groups were passivated by ethanolamine dissolved in water at 1 M concentration with the pH adjusted to 8.5. Based on our previous studies carried out for thicker hydrogel films, we assume that the hydrogel exposed to PBS swells and its thickness increases by a factor of ~ 9 (Wang et al., 2010). This results in the hydrogel layer thickness of $t_{\text{HG}} \sim 150$ nm and its refractive index of $n_{\text{HG}}=1.35$. Let us note that this surface architecture represents a versatile platform that was employed in immunoassays for the analysis of range of molecules in realistic samples. For instance, the NIPAAm-based hydrogel binding matrix was used for the detection of hormones (e.g., estradiol (Zhang et al., 2013)) in urine and other similar photocrosslinkable hydrogels were applied for surface plasmon-enhanced fluorescence detection of protein biomarkers (e.g. free prostate specific antigen-fPSA (Wang et al., 2009)) in blood serum. These assays can be readily combined with the presented BSW-enhanced fluorescence spectroscopy method.

2.4. Optical setup

In fluorescence assay experiments, an optical setup based on angular spectroscopy of BSWs and attenuated total reflection (ATR) was employed. This setup was derived from that described previously in more detail (Dostalek et al., 2007). As depicted in Fig. 1(b), a He-Ne laser beam at the excitation wavelength $\lambda_{\text{ex}}=633$ nm (that is close to the absorption band of used fluorophore labels $\lambda_{\text{ab}}=650$ nm) was launched into a 90° glass prism with a sensor chip optically contacted to its base. The laser beam was reflected from the prism base under an angle of incidence θ (taken in BK7 glass substrate) that was controlled by a rotation stage and its intensity was measured by a photodiode detector and a lock-in amplifier (Model 5210, Princeton Applied Research, USA). A transparent flow-cell with the volume of approximately $10 \mu\text{L}$ was attached to the sensor surface in order to flow liquid samples with target molecules with a flow rate of 0.503 mL/min by using a peristaltic pump (REGLO Digital

MS-4/12, ISMATEC, Switzerland). Fluorescence light emitted from affinity captured molecules into the aqueous medium was collected with a lens ($\text{NA}=0.3$) mounted above the flow-cell. The fluorescence intensity was measured in counts per second (cps) by a photomultiplier tube (H6240-01, Hamamatsu, Japan) which was connected to a counter (53131A, Agilent, USA). A set of filters including notch (XNF-632.8-25.0M, CVI Melles Griot, Germany) and band-pass (670FS10-25, LOT-Oriel, Germany) filters was used in order to suppress the background signal outside the emission wavelength $\lambda_{\text{em}}=670$ nm. For the observation of the dispersion relation of the BSWs supported by the 1DPC, angular reflectivity was measured at wavelengths between 600 and 700 nm. A collimated polychromatic light beam from a halogen lamp (LSH102, LOT-Oriel, Germany) was made incident on the sensor surface and the wavelength reflectivity spectrum was measured by using a spectrometer (HR4000 from Ocean Optics, USA) at angles of incidence between $\theta=40$ and 75 deg. (for more details see our previous work Toma et al. (2012)).

2.5. Modeling of 1DPC-mediated fluorescence

The Chance-Prock-Silbey model (Chance et al., 1978) was implemented in Mathematica (Wolfram Research, UK) scripts to simulate angular distribution of emitted fluorescence light intensity. Fluorophores were represented as an ensemble of randomly oriented dipoles located in the hydrogel matrix at a certain distance D from the surface of the 1DPC. The density of fluorescence intensity $F(\theta, \phi, D) d\theta \sin(\theta) d\phi$ emitted to polar θ and azimuth ϕ angles (in aqueous superstrate and BK7 glass substrate) was calculated as described in more detail in our previous work (Toma et al., 2011). By integrating $F(\theta, \phi, D)$, the emission probability F_{NA} within a numerical aperture $\text{NA}=0.3$ was determined. The emission probability from fluorophores homogeneously dispersed in the hydrogel matrix F_{HG} was obtained by averaging (see Supplementary materials). The electric field intensity $|E|^2$ distribution through the multilayer stack upon the resonant coupling to the BSW and the respective reflectivity were calculated by using home-developed Mathematica scripts based on the transfer-matrix method. RIs of Si-rich layer $n_{\text{H}}=2.381+0.0013i$ and $2.403+0.0013i$ were used at wavelengths λ_{em} and λ_{ex} , respectively. RIs of Si_3N_4 layer $n_{\text{L}}=1.784+0.0001i$ and $1.7844+0.0001i$ were assumed at wavelengths λ_{em} and λ_{ex} , respectively. RIs of BK7 glass $n_{\text{p}}=1.51$ and SU-8 film $n_{\text{SU8}}=1.6$ were used for both λ_{em} and λ_{ex} .

3. Results and discussion

3.1. Design and characterization of the 1DPC

The 1DPC structure was designed to enhance the field intensity at the fluorophore excitation wavelength $\lambda_{\text{ex}}=633$ nm and to block the propagation of emitted fluorescence light into the glass substrate at the emission wavelength $\lambda_{\text{em}}=670$ nm. In order to obtain such combined functionalities, the 1DPC comprises two segments S1 and S2, as described in the following. The design of the segment S1 was carried out to enable ATR-based coupling of a light beam to BSW at $\lambda_{\text{ex}}=633$ nm. In addition, the period of the S1 segment (230 nm) was tuned in such a way that no BSW exists at the emission wavelength $\lambda_{\text{em}}=670$ nm (see Supplementary materials, Fig. S1(a)). In doing so, we avoid unwanted BSW-coupled leakage of fluorescence emission through the substrate above the critical angle $\theta_{\text{c}}=61$ deg. at λ_{em} . In order to suppress the transmission of fluorescence light through the substrate at angles below the critical angle θ_{c} , an additional Bragg mirror segment S2 was employed. Its period (172 nm) was chosen in

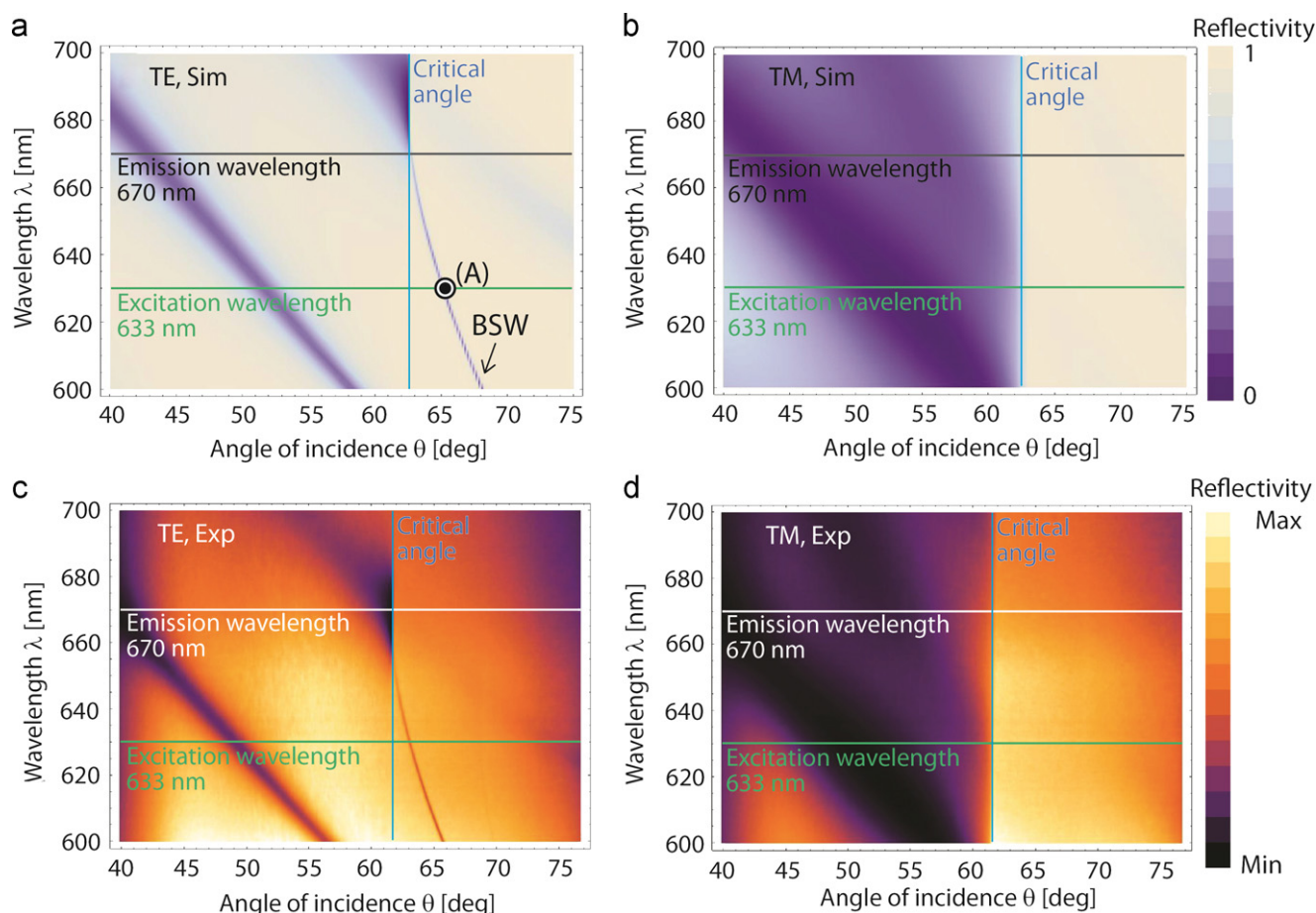


Fig. 2. Comparison of reflectivity map $R(\lambda, \theta)$ for the 1DPC obtained from (a), (b) simulations and (c), (d) experiments. The maps are shown for (a), (c) TE and (b), (d) TM polarization.

order to form a forbidden band below the light line at the emission wavelength λ_{em} (see Supplementary materials Fig. S1(b)). When the segments S1 and S2 are merged together in the 1DPC presented in Fig. 1, the resulting band structure is not the mere sum of those for separate S1 and S2 and a more complex behavior arises. In order to assess an insight on its optical response, reflectivity map $R(\lambda, \theta)$ from the 1DPC was calculated, see Fig. 2(a,b).

Fig. 2(a) and (b) reveal that the excitation of BSW (represented as a decrease in reflectivity) occurs only for the transverse electric (TE) polarized light beam that is incident at 1DPC through the prism at wavelengths $\lambda < 670$ nm above the critical angle $\theta > \theta_c$. The resonant coupling to BSW at λ_{ex} is associated with an extremely narrow resonance in the reflectivity spectrum exhibiting the angular width of $\Delta\theta = 0.1$ deg. (see the mark A in Fig. 2(a)). In addition, the reflectivity in the resonance reaches zero which indicates a full coupling of the incident light beam to BSW. At angles $\theta < \theta_c$, the expected high reflectivity provided by the Bragg mirror segment S2 is partially perturbed due to interference effects on merged 1DPC structure and owing to the disappearing BSW originating from the stack S1. The measured reflectivity from the fabricated 1DPC is presented in Fig. 2(c) and (d) for TE and transverse magnetic (TM) polarizations, respectively. These $R(\lambda, \theta)$ maps are in good agreement with simulations as the measured dispersion relation shows excitation of BSW mode only in TE polarization below the wavelength $\lambda < 670$ nm and reveals that no modes are supported in TM polarization. However, at the excitation wavelength λ_{ex} , the BSW resonance shows a broader angular width $\Delta\theta = 0.22$ deg. and a decreased coupling efficiency of $\sim 30\%$. This discrepancy can be ascribed to imperfections in

multi-layer stack fabrication and to an increase of losses due to surface scattering on roughness that was not taken into account in the model. Particularly, we assume that the random deviations in the thickness of individual layers forming the 1DPC stack leads to changed properties of BSW that are associated with the lower coupling efficiency.

As shown by simulations in Fig. 3, the resonant coupling to BSW on the top of the 1DPC structure at the excitation wavelength λ_{ex} and the angle of incidence $\theta = 64.45$ deg. (mark [A] in Fig. 2(a)) is accompanied with a strong electric field intensity. The electric field intensity $|\mathbf{E}|^2$ (normalized with that of the incidence beam $|\mathbf{E}_0|^2$) peaks at the interface between the 1DPC and the aqueous environment. The simulations predict that for the full coupling to BSW the maximum electric field intensity enhancement reaches $|\mathbf{E}/\mathbf{E}_0|^2 \sim 300$. The BSW evanescent field probes the aqueous medium on the top of the 1DPC with the penetration depth $L_p/2 = 166$ nm ($L_p/2$ is defined as the distance D at which the magnitude of electric field intensity $|\mathbf{E}/\mathbf{E}_0|^2$ decreases by a factor of $1/e$) that is comparable to the thickness of the attached hydrogel binding matrix $t_{HG} \sim 150$ nm. For comparison, the electric field intensity distribution was calculated for the total internal reflection (TIR) at the interface between a bare glass substrate and an aqueous medium (without the 1DPC layer structure). It shows that the maximum field intensity enhancement reaches a lower value of $|\mathbf{E}/\mathbf{E}_0|^2 \sim 4$ at the same angle of incidence $\theta = 64.45$ deg.

3.2. Fluorophore excitation mediated by 1DPC

Let us note that the excitation rate of a fluorophore label is (far from saturation) proportional to the electric field intensity $|\mathbf{E}|^2$ at

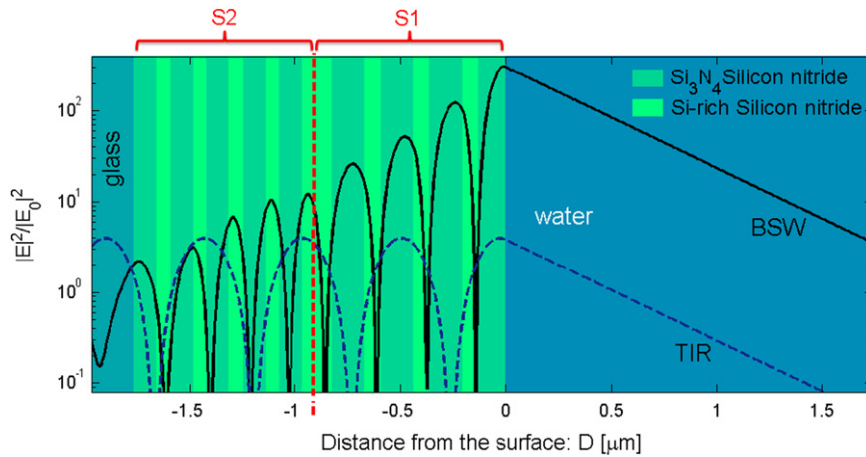


Fig. 3. Profile of electric field intensity upon the resonant coupling to BSW on the 1DPC (solid) compared to that for totally internally reflection at a glass–water interface (dashed). Angle of incidence is $\theta=64.45$ deg. for both structures.

the absorption wavelength λ_{ab} . Therefore, the strong electromagnetic field intensity provided by the excitation of BSW on the 1DPC is directly translated to the enhanced fluorescence signal emitted from the sensor surface. The above simulations indicate that the fluorescence excitation rate can be increased through BSW excitation on the 1DPC with respect to that for regular TIR by a factor of $\chi_{ex} \sim 75$ (defined as ratio of $|E/E_0|^2$ for the 1DPC and bare glass surfaces presented in Fig. 3). However, the wider BSW resonance and lower coupling efficiency observed on experimentally prepared 1DPC indicates that the enhancement factor χ_{ex} is smaller. Based on the fitting of measured reflectivity spectra by using a transfer-matrix model (data not shown), the peak field intensity enhancement of $|E/E_0|^2 \sim 20$ is predicted which results to a lower enhancement factor of $\chi_{ex} \sim 5$ with respect to TIR.

3.3. Fluorophore emission mediated by 1DPC

The angular distribution of fluorescence intensity can be controlled by the coupling of emitters with BSW or other types guided waves (Ballarini et al., 2011; Ganesh et al., 2008) and by the interference with back-reflected waves (Barnes, 1998). Further, we investigate the directionality of the fluorescence light emitted from the 1DPC that was designed to provide high reflectivity perpendicular to the surface. Fig. 4a compares the calculated polar angular dependence of the fluorescence intensity $F(\theta, \phi=0)$ emitted from the 1DPC structure and from a bare glass surface in contact with an aqueous medium. These data show that for the bare glass surface, the majority of fluorescence intensity is emitted into the glass with characteristic lobes in vicinity to the critical angle θ_c . From the glass surface with additional segment S1 (supporting BSW), a major fraction of emitted fluorescence intensity is also emitted into the glass substrate but that emitted toward the aqueous medium is slightly increased. With the additional segment S2 (serving as a Bragg mirror) placed below S1, the fluorescence intensity leaking into the substrate is strongly suppressed and highly directional emission toward the aqueous medium is observed. Depending on the distance D of a fluorophore from the surface, the emitted light that is back-reflected from the 1DPC structure gains a different phase-shift and thus the maximum intensity occurs at different polar angles (e.g., by changing the distance from $D=10$ to 140 nm the polar angle at which the maximum intensity occurs is shifted by ~ 18 deg.).

Based on these data, the emission probability of fluorescence light F_{NA} within the numerical aperture $NA=0.3$ was calculated. The results depending on the distance D are presented in Fig. 4b and show that F_{NA} oscillates with a period $\lambda_{em}/2n_s \sim 250$ nm and

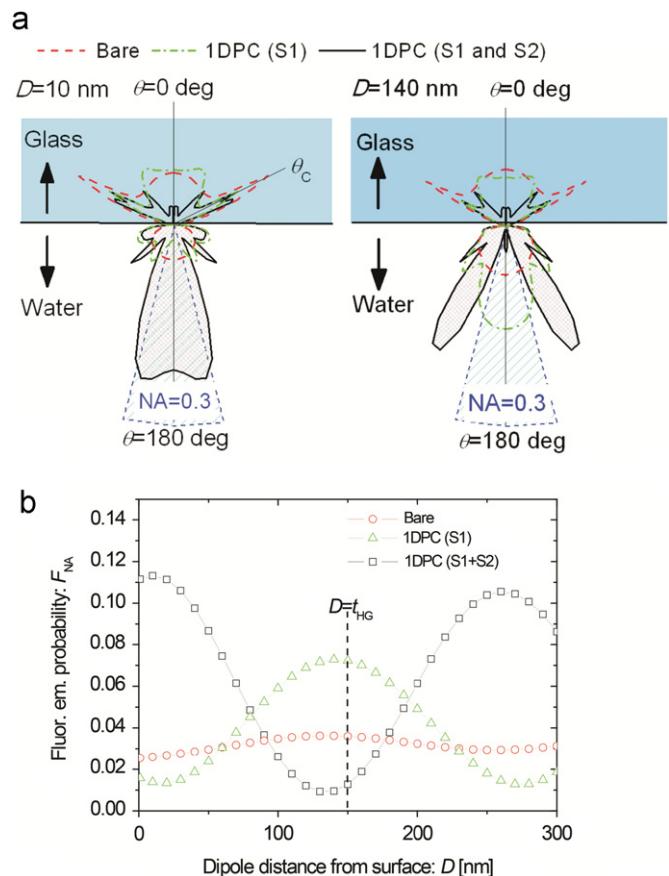


Fig. 4. (a) Normalized angular distribution of fluorescence intensity emitted by a randomly oriented dipole at the distance $D=10$ (left) and 140 nm (right) from the surface carrying 1DPC with the segments S1 and S2 (black solid line), 1DPC with the segment S1 (green dash dot line) and from a bare glass surface (red dash line) in contact with water. (b) Dependence of the fluorescence emission probability F_{NA} on the distance of a randomly oriented dipole from the sensor surface D . Simulations shown for 1DPC with (black squares) and without (green triangles) Bragg mirror segment S2, and for the reference bare glass substrate (red circles). (For interpretation of the references to color in this figure legend, the reader is referred to the web version of this article.)

reaches $F_{NA}=11\%$ for the 1DPC with both segments S1 and S2 and a distance of fluorophore from the substrate surface of $D=10$ nm. For 1DPC without the segment S2, a lower maximum emission probability $F_{NA}=7\%$ occurs at the fluorophore distance $D=140$ nm. On the bare glass surface, the maximum emission

probability reaches only $F_{NA}=4\%$ at the distance $D=140$ nm, which is about three-times lower than that for the 1DPC structure with both S1 and S2. Assuming that the binding of fluorophore-labeled molecules is homogeneously distributed within a hydrogel binding matrix with a thickness of $t_{HG}=150$ nm, the average emission probability F_{HG} from randomly dispersed fluorophores was obtained by integrating F_{NA} (see Supplementary materials). The calculated emission probability $F_{HG}=5.4\%$ is obtained for the whole 1DPC, which is higher than that for the bare glass surface $F_{HG}=3.2\%$. The predicted moderate enhancement of the collection efficiency by a factor of $\chi_{col}\sim 1.7$ (defined as the ratio of F_{HG} on the 1DPC and bare glass surfaces) is due to the rapid oscillation of the fluorescence intensity emitted to $NA=0.3$ with the distance D . A better collection enhancement (a factor up to $\chi_{col}\sim 4$) can be achieved for a thinner binding matrix (e.g. for the immobilization of capture molecules by using a monolayer-based surface architecture).

3.4. Model immunoassay experiment

Firstly, the angular reflectivity and fluorescence spectra were measured from the 1DPC and bare glass sensor chips carrying the hydrogel matrix. Fig. 5 shows that the coupling to BSW on the 1DPC surface is manifested as a resonant dip centered at the angle of incidence $\theta=63.21$ deg. The immobilization of mlgG molecules is associated with an increase of the refractive index n_H and leads to the shift of the resonance shifts to a higher angle $\theta=63.25$ deg. On the bare glass surface, no significant changes can be seen in the TIR angular spectrum before and after the immobilization of

mlgG molecules. After the affinity binding of fluorophore-labeled a-mlgG molecules, the fluorescence intensity F was measured as a function of the angle of incidence. For the 1DPC, a narrow peak occurs in $F(\theta)$ at the resonance angle $\theta=63.25$ deg, where the electric field intensity is enhanced by BSWs. In contrast, the fluorescence intensity peaks at the critical angle $\theta=61.7$ deg, and slowly decreases when increasing the angle of incidence for the reference bare glass surface.

In order to demonstrate the potential of the proposed 1DPC for signal amplification in fluorescence-based biosensors, a titration experiment was carried out. For the 1DPC, the angle of incident excitation laser beam ($\lambda_{ex}=633$ nm) was fixed at the BSW resonance $\theta=63.29$ deg, and the fluorescence signal F was measured in time upon the sequential flow of samples with a-mlgG molecules. The same angle of incidence was used for the TIRF readout on the reference bare glass sample. PBS-T samples with increasing concentration of a-mlgG were successively flowed along the sensor surface in order to bind to the surface. For the 1DPC chip, the a-mlgG concentration between 0.3 pM and 1 nM was used. For bare glass sensor chip, the analyte concentration was varied between 10 pM and 10 nM. Each sample was flowed over the surface with mlgG-functionalized hydrogel binding matrix for 10 min followed by 10 min rinsing with PBS-T. From the obtained a-mlgG affinity binding kinetics $F(t)$ on the 1DPC and reference bare glass sensor chips (shown in Fig. S2 in Supplementary materials), calibration curves were determined. A linear fit for association phase of the binding kinetics and the slope dF/dt was plotted as a function of a-mlgG concentration, see Fig. 6. The measurements were carried out in triplicate and the averaged calibration curves are shown with the error bars representing the standard deviation. We point out that this error is ascribed to the chip-to-chip variations and inaccuracy in incubation times. The limit of detection (LOD) was determined as the concentration at which the linear fit of the calibration curve crosses over the 3-fold standard deviation of the fluorescence signal for a blank sample σ . For the 1DPC sensor chip the $3\sigma=149$ cps/min was determined. This value is about 2.4 higher than that for the bare glass surface $3\sigma=62$ cps/min due the higher background signal. This effect is probably associated with stronger auto-fluorescence and scattering of light at the excitation wavelength upon the resonant coupling to BSW (see Fig. 5). The limit of detection of 2 pM was obtained for the sensor chip with the 1DPC, as compared to 25 pM for the regular bare glass.

The presented experiments reveal that the employment of the 1DPC allows enhancing the fluorescence intensity associated with the capture of target molecules on the sensor surface by a factor

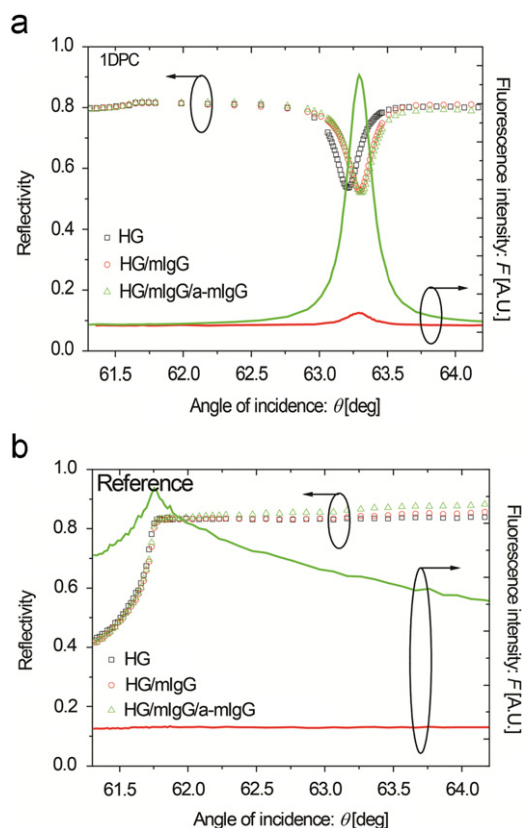


Fig. 5. Measured angular reflectivity and fluorescence intensity spectra for the sensor chip prior to the functionalization (black), after the covalent coupling of mlgG (red) and after the affinity binding of fluorophore-labeled a-mlgG (green). Data shown are (a) for the sensor chip carrying the 1DPC and (b) for the reference glass slide. (For interpretation of the references to color in this figure legend, the reader is referred to the web version of this article.)

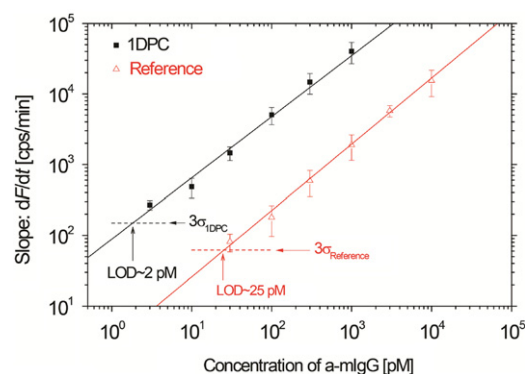


Fig. 6. Comparison of calibration curves for a-mlgG biosensor utilizing a fluorescence-based assay with BSW-enhanced detection on the 1DPC and with regular TIRF on bare glass slide. Calibration curves are fitted with a linear function and the baseline noise, error bars and LOD are clearly indicated.

of 30 with respect to regular TIRF. This enhancement translates to the improved limit of detection in the immunoassay-based analysis of molecular analyte by a factor of 12.5 (let us note that difference between the enhancement of the fluorescence intensity and the limit of detection is due to the increased background of fluorescence signal observed on the 1DPC). These values are significantly lower than those predicted by simulations which show that combining the improvement of collection efficiency $\chi_{\text{col}}=1.7$ and the increase of excitation rate $\chi_{\text{ex}}=75$ of fluorescence allows enhancing the sensor sensitivity by a factor of $\chi_{\text{col}}\chi_{\text{ex}}=127$. This discrepancy is due to the fact that the experimentally achieved field intensity enhancement is probably lower than expected from design, which leads to smaller factor $\chi_{\text{ex}}\chi_{\text{col}}=8.5$. Additional uncertainty is ascribed to the spatial distribution of captured a-mIgG in the binding matrix. Our previous works showed that the affinity binding of molecules in functionalized NIPAAm-based hydrogel occurs at the distance of few hundreds of nanometers from its interface with aqueous sample (Huang et al., 2010). However, the density of the hydrogel layer typically exhibits a gradient and the hydrogel is denser at the inner interface compared to that in contact with aqueous sample (Beines et al., 2007). Therefore, the capture of target analyte probably occurred preferably at the inner part of the hydrogel where the collection efficiency of fluorescence light is increased (see the comparison of fluorescence angular emission distribution in Fig. 4(a)).

4. Conclusions

A new one-dimensional photonic crystal (1DPC) that supports Bloch surface waves and serves as a Bragg mirror was investigated to advance the sensitivity in heterogeneous fluorescence assays for the detection of molecular analytes. The 1DPC was designed to amplify the fluorescence signal emitted from fluorophore labels by combining BSW-enhanced excitation rate and directional emission provided by a Bragg mirror. The theory predicts that this approach holds potential for increasing the sensitivity by more than two orders of magnitude with respect to regular TIRF. The experiments showed lower sensitivity enhancement by a factor of 12.5, mainly due to the imperfections of the prepared 1DPC. The future work will be devoted to further improve the design of 1DPC (e.g. by employing low auto-fluorescence materials and layer structure that is less sensitive to fabrication inaccuracies) and toward the implementation of this detection principle to microarrays detection formats.

Acknowledgments

Support for this work was partially provided by the Austrian NANO Initiative (FFG and BMVIT) through the NILPlasmonics

project within the NILAustria cluster (www.NILAustria.at), by the ESMI project, FP7-INFRASTRUCTURES-2010-1, Grant Agreement Number 262348 of the European Commission, and by the Italian MIUR Progetto Bandiera 2012 “NanoMax”.

Appendix A. Supplementary materials

Supplementary materials associated with this article can be found in the online version at <http://dx.doi.org/10.1016/j.bios.2012.12.001>.

References

- Aulasevich, A., Roskamp, R.F., Jonas, U., Menges, B., Dostalek, J., Knoll, W., 2009. *Macromolecular Rapid Communications* 30, 872–877.
- Ballarini, M., Frascella, F., Michelotti, F., Digregorio, G., Rivolo, P., Paeder, V., Musi, V., Giorgis, F., Descrovi, E., 2011. *Applied Physics Letters* 99, 043302.
- Barnes, W.L., 1998. *Journal of Modern Optics* 45, 661–699.
- Beines, P.W., Klosterkamp, I., Menges, B., Jonas, U., Knoll, W., 2007. *Langmuir* 23, 2231–2238.
- Descrovi, E., Sfez, T., Dominici, L., Nakagawa, W., Michelotti, F., Giorgis, F., Herzig, H.P., 2008. *Optics Express* 16, 5453–5464.
- Dostalek, J., Kasry, A., Knoll, W., 2007. *Plasmonics* 2, 97–106.
- Dostalek, J., Knoll, W., 2008. *Biointerphases* 3, Fd12–Fd22.
- Farmer, A., Friedli, A.C., Wright, S.M., Robertson, W.M., 2012. *Sensors and Actuators B* 173, 79–84.
- Ford, G.W., Weber, W.H., 1984. *Physics Reports* 113, 195–287.
- Fort, E., Grésillon, S., 2008. *Journal of Physics D* 41, 013001.
- Ganesh, N., Block, I.D., Mathias, P.C., Zhang, W., Chow, E., Malyarchuk, V., Cunningham, B.T., 2008. *Optics Express* 16, 21626–21640.
- García-Parajo, M.F., 2008. *Nature Photonics* 2, 201–203.
- Giannini, V., Fernández-Domínguez, A.I., Sonnefraud, Y., Roschuk, T., Fernández-García, R., Maier, S.A., 2010. *Small* 6, 2498–2507.
- Giljohann, D.A., Mirkin, C.A., 2009. *Nature* 462, 461–464.
- Guo, Y., Ye, J.Y., Divin, C., Huang, B., Thomas, T.P., Baker, J.R., Norris, T.B., 2010. *Analytical Chemistry* 82, 5211–5218.
- Huang, C.J., Dostalek, J., Knoll, W., 2010. *Biosensors and Bioelectronics* 26, 1425–1431.
- Chance, R.R., Prock, A., Silbey, R., 1978. *Advances in Chemical Physics*, 1–65.
- Lakowicz, J.R., Ray, K., Chowdhury, M., Szmacinski, H., Fu, Y., Zhang, J., Nowaczyk, K., 2008. *Analyst* 133, 1308–1346.
- Lazcka, O., Campo, F., Munoz, F.X., 2007. *Biosensors and Bioelectronics* 22, 1205–1217.
- Neumann, T., Johansson, M.L., Kambhampati, D., Knoll, W., 2002. *Advanced Functional Materials* 12, 575–586.
- Rivolo, P., Michelotti, F., Frascella, F., Digregorio, G., Mandracci, P., Dominici, L., Giorgis, F., Descrovi, E., 2012. *Sensors and Actuators B* 161, 1046–1052.
- Robertson, W.M., 1999. *Journal of Lightwave Technology* 17, 2013–2017.
- Robertson, W.M., May, M.S., 1999. *Applied Physics Letters* 74, 1800–1800.
- Shinn, M., Robertson, W.M., 2005. *Sensors and Actuators B* 105, 360–364.
- Sinibaldi, A., Danz, N., Descrovi, E., Munzert, P., Schulz, U., Sonntag, F., Dominici, L., Michelotti, F., 2012. *Sensors and Actuators B* 174, 292–298.
- Toma, K., Dostalek, J., Knoll, W., 2011. *Optics Express* 19, 11090–11099.
- Toma, M., Toma, K., Adam, P., Homola, J., Knoll, W., Dostalek, J., 2012. *Optics Express* 20, 14042–14053.
- Wang, Y., Brunsen, A., Jonas, U., Dostalek, J., Knoll, W., 2009. *Analytical Chemistry* 81, 9625–9632.
- Wang, Y., Huang, C.J., Jonas, U., Wei, T., Dostalek, J., Knoll, W., 2010. *Biosensors and Bioelectronics* 25, 1663–1668.
- Zhang, Q., Wang, Y., Mateescu, A., Sergelen, K., Kibrom, A., Jonas, U., Wei, T., Dostalek, J., 2013. *Talanta* 104, 149–154.